Structural Flexibility and the Thermodynamics of Helix Exchange Constrain Attenuation and Allosteric Activation of Hammerhead Ribozyme TRAPs†

Vanvimon Saksmerprome and Donald H. Burke*

Department of Chemistry, Indiana University, Bloomington, Indiana 47405-7102

Received June 4, 2003; Revised Manuscript Received September 25, 2003

ABSTRACT: Perturbations of precleavage equilibria in RNA-cleaving ribozymes can be exploited to control cleavage kinetics. In the targeted ribozyme-attenuated probes (TRAP) design, antisense and attenuator sequences are appended onto the catalytic core of a ribozyme or deoxyribozyme. The attenuator anneals to conserved bases in the catalytic core to form an inactive conformation, which is activated upon binding of a sense strand oligonucleotide to the antisense module. In this work, the apparent Michaelis-Menton constant (K'_m) for the binding of the RNA substrate to the ribozyme is shown to be within a factor of 2 for a number of constructs whose observed cleavage rates varied by several 100-fold. These observations rule out models of allosteric regulation based on modulation of substrate binding affinity, instead favoring a model in which regulation arises from equilibration between the active and inactive conformations of the TRAP. Free energies of formation for isolated helices that are exchanged during this reequilibration were determined from the concentration dependence of optical melt data. These values established that the thermodynamic stabilities of sense−antisense duplexes and of the attenuator-core duplexes correlate with observed rates of cleavage. Notably reduced cleavage rates are observed for TRAP ribozymes with extended antisense sequences, suggesting that tight binding of attenuator to the core is assisted by a long antisense portion. A construct with a 25-nucleotide antisense showed greater than 730-fold activation upon annealing with a 20-nucleotide DNA sense strand oligo, representing the greatest activation observed to date for the TRAP design.

Allostery has long been recognized as a powerful mechanism for real-time regulation of enzyme activity in response to changing concentrations of cellular components. Allosteric ribozymes and deoxyribozymes are nucleic acid enzymes that have been engineered or selected in vitro to be either activated or repressed upon binding a given effector molecule, such as an organic species, a peptide, a protein, or an oligonucleotide (*1*, *2*). As sensors, these molecular switches have been decorated with fluorescent dyes for the detection of small organic analytes (*3*, *4*) and metal ions (*5*). As potential therapeutic agents, their abilities to cleave a target mRNA can be similarly governed by effector molecules, and at least one such design has shown efficacy inside mammalian cells (*6*).

TRAP[1] ribozymes are targeted ribozyme attenuated probes (*7*). In the TRAP design, two sequence modules are appended onto one end of a known (deoxy)ribozyme. The distal module ("attenuator") contains sequences that can base pair with the catalytic core of the ribozyme (Figure 1). In the case of hammerhead TRAP ribozymes, this pairing shuts down cleavage of the RNA target by the hammerhead. The proximal module ("antisense") acts as a flexible tether. Binding of a "sense" strand to the antisense straightens and stiffens the tether, preventing attenuation and activating cleavage of substrate RNA. This design makes cleavage of a target RNA by the ribozyme dependent upon the presence of a third RNA strand that acts as activator. One possible application of this design is to induce cell killing by cleaving an mRNA for an essential protein, but only do so in cells that express an RNA that indicates a pathological state, such as viral RNA or a tumor-associated mRNA. The specificity of cleavage and activation can be programmed in interchangeable modules without some of the sequence constraints that accompany some other allosteric ribozyme designs, so long as internal structure does not interfere with attenuation or activation.

A thorough understanding of the parameters that govern TRAP reactivity would aid in the design of allosteric ribozymes for gene therapy, biosensors, and other applications. We have proposed that TRAP kinetics are primarily governed by the relative stabilities of the activation and attenuating helices (*7*), but other mechanistic models are also possible. For example, while the TRAP design is not intended to affect substrate binding affinity, formation of a productive E·S complex could, in principle, be limited by decreased affinity for the RNA substrate by the attenuated ribozyme. This would result in lower concentrations of E·S complex, and thereby a lower observed rate of cleavage. Displacement of the attenuator from the core would then activate cleavage by restoring affinity for the substrate. Similarly, the length

† This work was supported by NIH Grant AI45344 and a Beckman Young Investigator Award to D.H.B. and by a graduate research fellowship from the Royal Thai Government to V.S.

* Corresponding author: tel: 812-856-4977; fax: 812-855-8355; E-mail: dhburke@indiana.edu.

[1] Abbreviations: TRAPs, targeted ribozyme attenuated probes; E, active form of enzyme; E*, attenuated (inactive) form of enzyme; S, substrate; k_{obs}, observed cleavage rate; K'_m, apparent Michaelis−Menten constant; K_d, dissociation constant.

10.1021/bi034960k CCC: $25.00
Published on Web 11/05/2003

FIGURE 1: Hammerhead TRAPs. (A) Schematic representation of TRAP activation through binding of a sense strand oligonucleotide. Green and red lines correspond to strands that interact in the "off" state (E*). Pairing of a sense activator with the antisense (blue line) should activate the hammerhead (E) to cleave its substrate (S). The cleavage site in the substrate strand is shown as a block arrow. Structural features involved in allostery are indicated. (B) Nucleotide sequences of TRAPs and activating oligos used in determination of K'_m for cleavage substrate. Following the color scheme used in panel A, attenuator sequences and their binding target in the core shown in lower case, cleavage substrate in large bold with cleavage site indicated. The longer attenuator corresponds to that of HH8A.10, the shorter one to that of HH8A.8, and HH8A carries no attenuator.

of the antisense segment could limit the attenuator's ability to reach the core, thus affecting the kinetic behavior of the attenuated TRAP.

The present work examines the effects of substrate binding affinity, duplex thermodynamics, and antisense length on precleavage equilibria and kinetics for hammerhead TRAP ribozymes. We find that affinity for substrate is not significantly affected by attenuation or activation, that cleavage rates correlate directly with thermodynamic stabilities of activating duplexes and inversely with those of attenuator−core duplexes, and that flexibility and length of the antisense segment strongly influence observed cleavage rates.

EXPERIMENTAL PROCEDURES

Ribozymes, RNA Substrate, and Oligonucleotides. DNA and RNA oligonucleotides were chemically synthesized by Integrated DNA Technologies (Coralville, IA) or by Dharmacon (Lafayette, CO). Ribozymes were transcribed in vitro from synthetic templates, radiolabeled, and purified as described (*7*).

Determination of Apparent Michaelis-Menton Constants (K'_m) and First-Order Rate Constants (k_{obs}). For K'_m determination, multiple turnover reactions were carried out with excess substrate (10−200 nM) over ribozyme (1 nM). Activating oligonucleotides, when used, were at saturating concentrations in the range of 40 nM to 1 μM. Ribozyme, end-labeled substrate and activator (if used) were heated at 90 °C for 1 min in 50 mM Tris-HCl, pH 7.5 and slowly cooled to room temperature on the bench top for 5 min. Reactions were initiated by the addition of $MgCl_2$ to a final concentration of 10 mM. Aliquots were removed at appropriate time intervals and quenched with stop buffer (50 mM EDTA, 8 M urea, 10% sucrose, 35% glycerol, 0.5% bromophenol blue, and 0.5% xylene cyanol). Samples were analyzed by denaturing (7 M urea) 12% PAGE. Cleaved and uncleaved substrate bands in the gels were quantified using the ImageQuant software from Molecular Dynamics. Initial velocities were determined for each substrate concentration from a best-fit line, typically based on six data points obtained over the first 10% of the reaction. K'_m values were determined from best-fit lines in Eadie-Hofstee plots of v_o/[enzyme] vs (v_o/[enzyme])/[substrate]. For determination of apparent k_{obs}, single turnover reactions were conducted as above, but with ribozyme (2 μM) in excess of substrate (0.2 μM). Activating oligonucleotide of 6 μM, if used, was added prior to the heating and refolding steps. Experimental k_{obs} values (average of at least two independent experiments) were determined from the slope of the intial values in a plot of ln(fraction uncleaved) vs time, using the linear range after any short burst phase (usually corresponding to less than 10% of total material).

Thermodynamic Analysis. Concentration of each RNA or DNA strand was calculated from UV absorbance (260 nm) at 25 °C. There was no apparent melt behavior when oligos were heated separately in the standard kinetic buffer. Therefore, we take the 25 °C absorbance data to reflect that of the single-stranded state. RNA/DNA and RNA/RNA duplexes were heated to 90 °C, and then allowed to cool slowly to room temperature on the bench top for 5 min in the buffer as described above. Absorbance versus temperature melting curves were measured at 260 nm with a heating rate of 0.5C°/min over the temperature range 25−85 °C on a Cary100 Bio UV−visible spectrophotometer equipped with a Peltier heating/cooling accessory and a temperature probe. Melting temperature (T_m) was obtained as the maximum value in plots of dAbs(260)/dT vs T. Note that T_m as the maximum in first derivatives only applies to large ΔH values (for a two-state transition) (*8*), a criterion that is amply met by the data presented here. The dependence of T_m on strand concentration was analyzed to yield ΔH and ΔS for the transition from duplex to single strand involving non-self-complementary sequences: $1/T_m = R/\Delta H \ln C + (\Delta S - R \ln 4)/\Delta H$, where C is the sum of molar concentrations of each strand and R is the gas constant (*9*). $\Delta G_{25°C}$ was calculated from $\Delta G_{25°C} = \Delta H - T\Delta S$. Errors of the thermodynamic parameters were propagated using standard methods from the uncertainties in the slope and y-intercept in plots of the equation above.

RESULTS

Attenuation Does Not Interfere with Substrate Binding. Substrate cleavage by hammerhead TRAP ribozymes is repressed due to the presence of an attenuator sequence capable of base pairing with the catalytic core. To determine

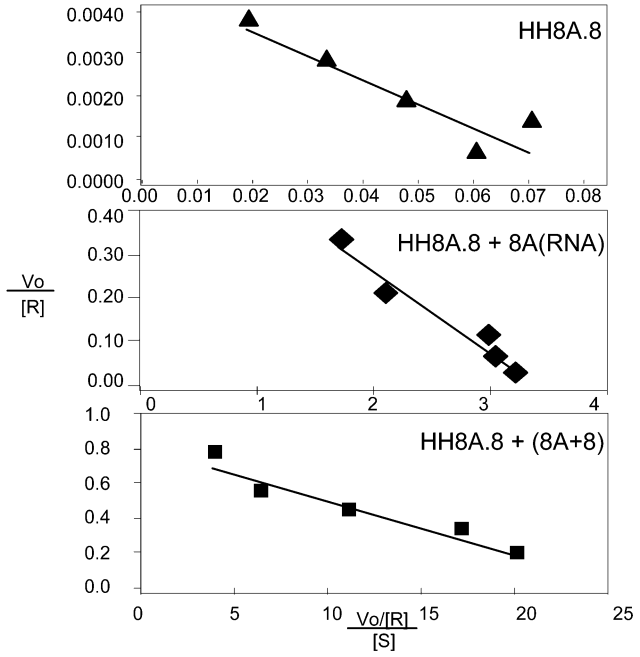

FIGURE 2: Determination of apparent Michealis-Menton constants (K'_m) using Eadie-Hofstee plots, in which initial cleavage rates normalized to ribozyme concentration (v_o/[R], in units of min^{-1}) are plotted as a function of this normalized rate divided by substrate concentration in μM. Data are plotted for HH8A.8 alone (top), for HH8A.8 in the presence of sense strand oligo 8A (middle), and for HH8A.8 in the presence of anti-attenuator oligo 8A+8 (bottom).

whether attenuation interferes with binding of the RNA substrate, we determine the affinity of the ribozyme-substrate interaction by comparing equilibrium dissociation constants (K_d) of attenuated ribozymes to those of nonattenuated constructs. The ribozymes chosen for this study are shown in Figure 1. The kinetic behavior of hammerhead HH8 has been analyzed in both single- and multiple turnover formats (*10*, *11*). Hammerheads HH8A, HH8A.8, and HH8A.10 are TRAP derivatives of HH8 carrying a 20-nt antisense segment (the "A" designation) in combination with attenuators of lengths 0, 8, or 10 nucleotides, respectively (the ".8" and ".10" designations).

Electrophoretic mobility shifts of radiolabeled substrate RNA (13 nt) on native polyacrylamide gels in the presence of variable concentrations of HH8 gave an apparent K_d of approximately 50 μM (not shown). This value is more than 1000-fold higher than expected from previous reports (*10*, *11*), and appears to result from dissociation of the complex during electrophoresis, as longer gels gave notably less shifted product than shorter gels. The native gel mobility shift method is therefore unsuitable for obtaining an accurate K_d for this substrate RNA. Because dissociation of both substrates and products is fast relative to the cleavage rate for most hammerhead ribozymes (*10*−*13*), the apparent Michaelis-Menton constants (K'_m) obtained under multiple-turnover conditions (substrate excess) is approximately equal to k_{-1}/k_1. Eadie-Hofstee plots of initial rates of substrate cleavage (v_o) gave reproducible K'_m values that serve as surrogates for the dissociation constant K_d (Figure 2).

Hammerhead HH8 yielded a K'_m value of 31 ± 10 nM (Table 1), which is in close agreement with published values of 41 and 49 nM for this ribozyme-substrate pair (*10*, *11*). The K'_m of hammerhead HH8Ais only slightly higher at 63 ± 4 nM. As the single-turnover cleavage rate of HH8A is indistinguishable from that of HH8 (*7*), the A-rich antisense segment has no effect on either equilibrium substrate binding or on cleavage kinetics. Single turnover cleavage rates for HH8A.8 and HH8A.10 are reduced by approximately 300−1000-fold relative to that of HH8 (Table 1) (*7*). Nevertheless, K'_m values measured for these species were 45 ±13 and 39 ± 15 nM, again similar to that of HH8. Annealing of attenuator to the catalytic core therefore does not diminish the affinity of attenuated ribozyme for substrate.

Table 1: Michaelis-Menton Constants for Substrate-Hammerhead TRAPs

hammerhead	activator oligo	K'_m (nM)[a]	k_{obs}[b] (min^{-1})	k_{rel}[c]
HH8	none	31 ± 10	0.6 ± 0.1	
HH8A	none	63 ± 4	0.63 ± 0.02	1
HH8A	8A(RNA)	35 ± 9	1.18 ± 0.03	2
HH8A.8	none	45 ± 13	0.0024 ± 0.0002	1
HH8A.8	8A(DNA)	n.d.	0.45± 0.01	190
HH8A.8	8A(RNA)	121 ± 35	0.65 ± 0.02	270
HH8A.8	8A+8(DNA)	26 ± 5	0.86 ± 0.07	360
HH8A.10	none	39 ± 15	0.0005 ± 0.0001	1
HH8A.10	8A(DNA)	n.d.	0.0074 ± 0.0005	15
HH8A.10	8A(RNA)	96 ± 39	0.13 ± 0.08	270
HH8A.10	8A+10(DNA)	84 ± 20	0.88 ± 0.02	1760

[a] K'_m values obtained from Eadie-Hofstee plots as in Figure 2. [b] Values of k_{obs} from measurements of single-turnover reactions (8). [c] Relative cleavage rates normalized to rate observed in the absence of activating oligo for a given ribozyme.

Activation Has Modest or No Effect on Substrate Binding. Addition of a sense strand activator oligonucleotide "8A" complementary to the antisense segment, or of an oligonucleotide complementary to both the antisense and attenuator portions (such as "8A+8"), stimulates cleavage by attenuated TRAP constructs to near the rate of HH8 (*7*). The K'_m values for ribozymes HH8A.8 and HH8A.10 in the presence of anti-attenuator oligos 8A+8 and 8A+10 are not significantly different from that of HH8. In contrast, the K'_m values for HH8A.8 and HH8A.10 in the presence of RNA oligo 8A are 2−3-fold higher than the values measured for the same ribozymes without activating oligo. To determine whether this effect is due to the use of 8A as the activator oligo or to the presence of the attenuator sequence in the ribozyme, K'_m values were obtained for hammerhead HH8A, which contains the same antisense sequence as HH8A.8 and HH8A.10, but lacks attenuator sequences (Table 1). The value of K'_m obtained for HH8A in the presence of RNA oligo 8A (35 ± 9 nM) is close to those observed for HH8 and for HH8A in the absence of an activator oligo. The slight reduction in affinity for substrate observed for HH8A.8 and HH8A.10 in the presence of RNA oligo 8A is thus due to contributions from the attenuator sequences, rather than to the sense-antisense interaction. While the mechanistic basis of this K'_m effect is not immediately apparent, it is possible that transient formation of the attenuator−core duplex may force stem III to fray slightly to accommodate geometric constraints, reducing the average number of paired bases and raising K'_m. This scenario would not arise with the anti-attenuator oligos both because the attenuator is tied up in base-paired interactions with the oligo and because the 8−10 unpaired bases at the 5′ end of the antisense segment could provide the conformational flexibility to relieve the geometric constraints. In sum, the similar K'_m values measured here

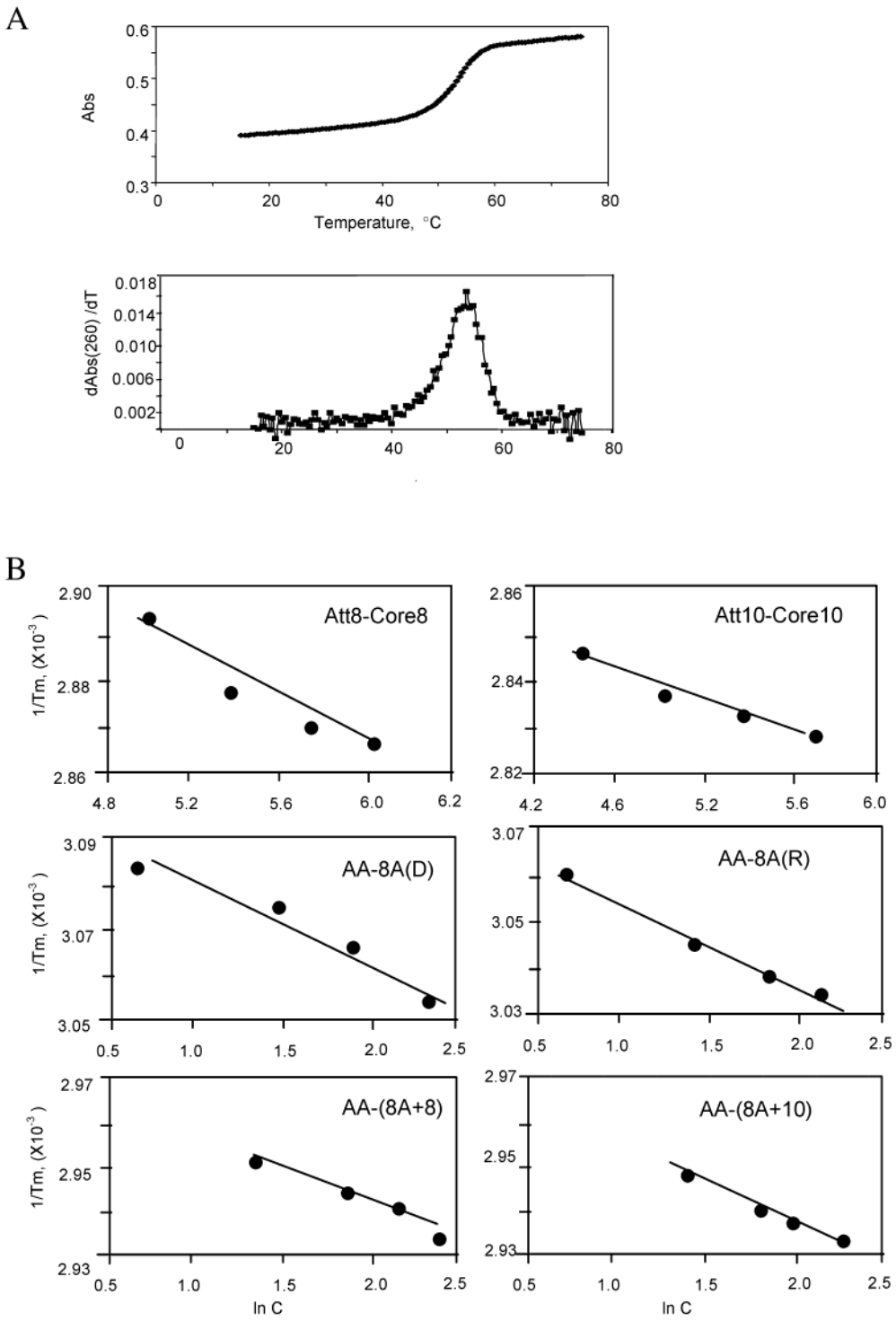

FIGURE 3: Thermodynamic determinations. (A) representative plot showing temperature dependence of absorbance at 260 nm of AS(R)-8A(R) duplex in Tris-Mg^{2+} buffer, pH 7.5 (top). Melting temperature, T_m, of the duplex was obtained as the maximum value in plot of dAbs(260)/dT vs temperature (bottom). (B) Thermodynamic analysis of the duplexes indicated using van't Hoff plots, using same buffer as in A. Abbreviations are as in Table 2. Oligonucleotide concentrations were 100−400 μM for top two plots and 2−10 μM for bottom four plots.

rule out models of attenuation (or activation) based on perturbations (or restoration) of substrate binding affinity.

Free Energies of Sense-Antisense and Attenuator-Catalytic Core Interactions. Competition between the sense−antisense duplex and the attenuator−core duplex is expected to be an important factor regulating cleavage kinetics of TRAP ribozymes. Consequently, the thermodynamic stabilities of these two interactions should correlate both with the degree of attenuation and with the degree of activation by appropriate oligonucleotides. Preliminary data using RNA vs DNA oligonucleotides gave qualitative support for this hypothesis (*7*), but did not evaluate free energy explicitly. Temperature-dependent melting behaviors offer a convenient means by which to evaluate thermodynamic parameters. Because such transitions can be obscured by other melt transitions within the context of attenuated hammerheads, thermal melt transi-

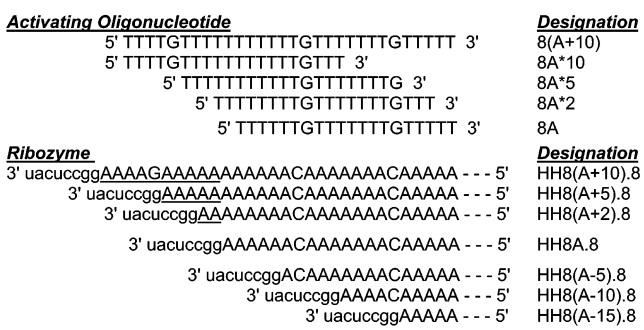

FIGURE 4: Constructs used to evaluate effects of antisense length and location of single-strandedness. Five activating DNA oligonucleotides are shown above, aligned with their binding targets in the ribozymes below. All ribozymes are derivatives of HH8A.8. Attenuators are shown in lower case; nucleotides inserted into the 3′ end of the antisense relative to HH8A.8 are underlined.

Table 2: Thermodynamic Parameters for Oligonucleotide Duplexes

Duplex	Designation [a]	ΔH (kcal/mol)	ΔS (cal/(mol•degree))	ΔG_{37C} (kcal/mol)
Attenuation Models				
5' AUGAGGCC 3' 3' UACUCCGG 5'	Att8 – Core8	-90 ± 16	-268 ± 54	-10 ± 3
5' UGAUGAGGCC 5' 3' ACUACUCCGG 3'	Att10 – Core10	-105 ± 7	-305 ± 20	-14 ± 1
Activation Models				
5' TTTTTTGTTTTTTTGTTTTT 3' 3' AAAAAACAAAAAAACAAAAA 5'	AS – 8A	-90 ± 23	-278 ± 70	-7 ± 2
5' UUUUUUGUUUUUUUGUUUUU 3' 3' AAAAAACAAAAAAACAAAAA 5'	AS – 8A	-117 ± 8	-356 ± 23	-11 ± 1
5' ATGAGGCCTTTTTTGTTTTT 3' 3' ACUACUCCGGAAAAAACAAAAA 5'	AA – (8A+8)	-110 ± 23	-238 ±59	-13 ± 5
5' TGATGAGGCCTTTTTTGTTT 3' 3' ACUACUCCGGAAAAAACAAAAA 5'	AA – (8A+10)	-153 ± 8	-451 ± 22	-18 ± 1

[a] Designations are in the form of (bottom strand)−(top strand). Abbreviations: Att8, 8-nt attenuator; Core8 and Core10, 8- or 10-nt segment from catalytic core; 8A(R), RNA version of 8A;8A(D), DNA version of 8A; AS, antisense; AA, binding target for antiattenuator oligo including antisense and 10-nt attenuator (cf., Figure 1); 8A+8 and 8A+10, antiattenuator oligos. Calculations for thermodynamic parameters are described in Material and Methods.

tions were monitored for DNA−RNA and RNA−RNA duplexes that mimic sense−antisense and attenuator−core helices in HH8A.8 and HH8A.10 (Figure 3). Comparing the thermodynamic parameters summarized in Table 2 with observed cleavage rates given in Table 1 shows that TRAPs carrying more stable attenuators cleave substrate more slowly than TRAPs with less stable attenuators, while activator oligos that form more stable duplexes restored activity to a greater degree than oligos that form less stable duplexes. Thus, the trends in kinetic behavior can be predicted in part from the thermodynamic stabilities of the individual duplexes.

Antisense Length and Flexibility Affect Cleavage Kinetics of Attenuated Ribozymes. Because the antisense segment must tether stem III to the attenuator−core duplex for attenuation to occur, the length and conformational flexibility of the antisense segment could influence attenuation of TRAP ribozymes. To investigate these parameters, single-turnover cleavage rates were measured for attenuated ribozymes with antisense segments extended by the insertion of 2, 5, or 10 nucleotides between the antisense and attenuator of HH8A.8 to generate species HH8(A+2).8, HH8(A+5).8, and HH8(A+10).8 (Figure 4). HH8(A+2).8 exhibits single-turnover cleavage that is approximately 3-fold faster than that of HH8A.8, while HH8(A+5).8 is approximately 3-fold slower. No cleavage is observed by HH8(A+10).8 (Table 3). The decline in cleavage activity at the two longest antisense lengths may result from a reduction in structural constraints as more nucleotides are added, allowing the attenuator better access to the core and favoring the inactive attenuated conformation.

Two types of activators were used to rescue the cleavage activity of these ribozymes. Annealing of oligo 8A, which interacts only with the original 20-nt antisense portion, leaves the 3′ ends of the antisense region unpaired, permitting evaluation of the effect of flexibility at that end. In contrast, activating oligos 8A*2, 8A*5, and 8A*10 pair with the 3′ terminal 20 nucleotides of the antisense, leaving 2, 5, or 10 nucleotides of the 5′ end of the antisense segment single-stranded (Figure 4). When 8A was added into the reaction containing HH8(A+2).8, single-turnover cleavage was restored to 0.88 min^{-1}. This 230-fold allosteric rate enhancement is similar to that observed previously for HH8A.8 (*7*). Addition of the activating oligo 8A*2 resulted in a k_{obs} similar to the reaction activated by the DNA sense oligo 8A. For HH8(A+5).8, the observed rate constants in the presence of oligos 8A and 8A*5 were 0.25 and 0.33 min^{-1}, respectively. Single-stranded segments of 2−5 nucleotides at either end of the antisense therefore have little effect on activation by a sense-strand oligo. However, the values for activated HH8(A+5).8 in the presence of oligos 8A and 8A*5 are 555- and 733-fold faster than the cleavage rate in the absence of the activating oligos, representing the greatest degree of activation yet observed for the allosteric TRAP design. In this case, the increased degree of activation is due to a greatly diminished cleavage rate for the unactivated ribozyme, even though the activated rate is still significantly below the maximal cleavage rates.

Neither oligo 8A nor 8A*10 rescues the cleavage by HH8(A+10).8 to detectable levels (<0.0004 min^{-1}), even during 1-h cleavage reactions. These 20-nt oligos leave 10 nucleotides unpaired at one end or the other of the antisense. This configuration may make it possible for the sense−antisense, attenuator−core, and stem III duplexes to coexist, removing the driving force toward refolding into the active conformation. To test this hypothesis, a longer activator oligo, "8(A+10)," which can pair directly with the entire 30-nt antisense sequence, was used to activate the cleavage reaction. In the presence of oligo 8(A+10), hammerhead HH8(A+10).8 cleaves its substrate with k_{obs} of 0.12 min^{-1}. The value is at least 300-fold above the unactivated rate, although the actual degree of activation may be much greater.

Attenuation in Ribozymes with Shortened Antisense Segments. To examine ribozyme attenuation in the context of TRAPs carrying truncated antisense segments, 5, 10, or 15 nucleotides were removed from the 3′ end of the antisense portion of HH8A.8 while leaving the attenuator intact to yield HH8(A-5).8, HH8(A-10).8, and HH8(A-15).8. We had originally hypothesized that a very short antisense region might not permit the attenuator to reach the catalytic core, thereby preventing attenuation. However, cleavage by each ribozyme is notably attenuated, with observed rates that are only slightly different from that of HH8A.8 (Table 3). The basis for this attenuation is unclear, although we note that five nucleotides in the attenuator can pair with a segment of stem II (GGCCU/AGGCC) and prevent its formation. The potential for similar interaction in other constructs can be safely ignored, as in those instances the attenuator is eight

Table 3: Initial Cleavage Rates for TRAP Ribozymes with Various Lengths of Antisense

hammerhead	activator[a]	length of oligo (nt)	k_{obs} (min^{-1})[b]	degree of activation[c]
HH8A.8	none		0.0012	
HH8(A+2).8	none		0.0038 ± 0.0002	1
HH8(A+2).8	8A	20	0.88 ± 0.15	231
HH8(A+2).8	8A*2	20	0.76 ± 0.14	200
HH8(A+5).8	none		0.00045 ± 0.00007	1
HH8(A+5).8	8A	20	0.25 ± 0.00[d]	555
HH8(A+5).8	8A*5	20	0.33 ± 0.01	733
HH8(A+10).8	None		<0.0004[e]	
HH8(A+10).8	8A	20	<0.0004[e]	
HH8(A+10).8	8A*10	20	<0.0004[e]	
HH8(A+10).8	8(A+10)	30	0.13 ± 0.01	>325
HH8(A-5).8	none		0.0009	
HH8(A-10).8	none		0.0028 ± 0.0004	
HH8(A-15).8	none		0.0013 ± 0.0001	

[a] All activators here are DNA oligonucleotides. [b] Single-turnover cleavage rates at saturating concentrations of ribozyme. Each k_{obs} is an average number from two kinetics assays. [c] Relative to same ribozyme without activating oligo. [d] Both measurements were identical, such that systematic error of measurement is <0.00 min^{-1}. [e] No cleavage detected; rate is less than the detection threshold of approximately 0.0004 min^{-1}.

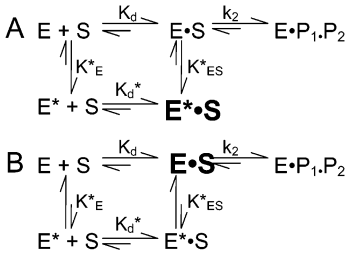

FIGURE 5: Kinetic scheme for RNA cleavage by hammerhead TRAP ribozymes without (A) or with (B) activating oligo. E, active state of ribozyme; E*, inactive state formed upon binding of the attenuator to the core. Majority species in the equilibria are shown in bold.

nucleotides in length and presumably offers a more stable interaction than this potential secondary attenuation site. The possibility of intermolecular inhibition was also considered, wherein two or more hammerhead molecules associate to form mutually inhibitory structures. Substrate cleavage by HH8(A-15).8 was not affected by doubling its concentration from 1 μM (the concentration used in all single-turnover assays above) to 2 μM, suggesting that intermolecular inhibition is not responsible for the attenuation in ribozymes with truncated antisense sequences. However, as the concentration of HH8(A-15).8 was further increased to 4 or 8 μM, cleavage rates decreased from 0.0014 min^{-1} to less than 0.0004 per min^{-1} (data not shown). Potential inhibitory interactions among hammerhead molecules should thus be taken into consideration for applications that call for high ribozyme concentrations.

DISCUSSION

Precleavage Equilibria. The present work examines the effects of substrate binding affinity, duplex thermodynamics, and antisense length on precleavage equilibria and kinetics for hammerhead TRAP ribozymes. The similarities among K'_m values derived from Eadie-Hofstee plots demonstrate that affinity for substrate is not affected by attenuation or activation in a way that could account for the observed cleavage rates. In the kinetic schemes shown in Figure 5, these results imply that $K_d \approx K^*_d$. To complete the thermodynamic cycle, the equilibrium between the active (E) and attenuated (E*) conformations of the ribozyme when substrate is bound (K^*_{ES}) must be approximately isoenergetic with this equilibrium in the absence of substrate (K^*_E). The fact that $K_{ES} \approx K^*_{ES}$ suggests that the TRAP ribozymes can be thought of as undergoing a classical noncompetitive inhibition, and that variations on the equations describing noncompetitive inhibition could apply to this system.

Ribozymes that carry attenuators exist predominantly in the E*·S form (Figure 5A). Addition of an activator oligonucleotide stabilizes the E·S form relative to E*·S (Figure 5B). The fraction of ribozyme−substrate complex in the active E·S conformation is expected to reflect the free energy difference between E and E* ($\Delta\Delta G_{activation}$), which is expected, in turn, to be reflected in net cleavage rates. In this simple model, $\Delta\Delta G_{activation} = \Delta G_{attenuated\ state} - \Delta G_{activated\ state} = -RT \ln(k_{attenuated}/k_{activated})$. The thermodynamic data in Table 2 correlate with several trends observed in TRAP ribozyme kinetics. First, the ten-base-pair duplex corresponding to the attenuator−core interaction in HH8A.10 is more stable than the corresponding eight-base-pair duplex derived from HH8A.8, in agreement with previous observations that HH8A.10 cleaves substrate more slowly than HH8A.8 (*7*). The additional stabilization energy in HH8A.10 is interpreted as maintaining the complex in the attenuated form a greater fraction of the time. Second, the activating oligo 8A stimulates the cleavage activity of HH8A.10 to a greater extent if provided in RNA form than in DNA form (*7*). We have speculated that this difference arises from a greater stability generally observed for RNA−RNA helices than for RNA−DNA helices (*14*−*17*), and the values measured here suggest approximately 4 kcal/mol difference in free energy between the two duplexes when measured in isolation ($\Delta G_{AS(R)-8A(D)}$ vs $\Delta G_{AS(R)-8A(R)}$, Table 2). Third, cleavage by HH8A.8 and HH8A.10 is stimulated to a greater degree by oligonucleotides that include complementarity to the attenuator sequences than by oligonucleotides that are complementary only to the antisense (*7*). Even though all stimulating oligonucleotides used in the earlier study were 20 nucleotides in length, the anti-attenuator oligonucleotides carry a higher G+C content than oligo 8A. Duplexes formed by anti-attenuator DNA oligonucleotides 8A+8 and 8A+10 with their complementary RNA strands are considerably more stable than helices involving oligo 8A (Table 2). We

conclude that the greater kinetic activation conferred by the anti-attenuator oligos is due to their greater stability, and does not result simply from pairing with the attenuator.

The value of $\Delta\Delta G_{activation}$ may be best described as the sum of the free energy contributions for each component of the structural rearrangement, such that $\Delta\Delta G_{activation} = \Delta G_{unfold\ attenuator-core} + \Delta G_{form\ sense-antisense} + \Delta G_{reform\ stem\ II} + \Delta G_{refold\ core} + \Delta G_{conformational\ constraints}$. Approximate values for the first and second terms are given in Table 2. The third and forth terms contribute approximately −9.6 kcal/mol (calculated from mfold (http://bioinfo.math.rpi.edu/~zuker-m)) and +3 to +7 kcal/mol (*12*, *13*). The value of $\Delta G_{conformational\ constraints}$ is more difficult to estimate, although conformational constraints in the attenuated state will contribute positive free energy that depends on antisense length. This is most evident in the constructs with extended antisense sequences, which were markedly more attenuated than HH8A.8 even though the helices exchanged during activation were identical. The trends noted above are in qualitative agreement with this analysis. To arrive at quantitative predictions of cleavage rates from this equation, it is important to keep in mind that once annealing a given oligo converts the majority of the ribozymes into the active conformation, further stabilization of the active conformation may have little effect. Furthermore, uncertainties in the precise values of the calculated ΔG values are amplified when differences between them are calculated to arrive at $\Delta\Delta G_{activation}$ values.

Length and Flexibility of Antisense Alter Repressibility and Activation of TRAP Ribozymes. There would be no allosteric activation if the sense−antisense, attenuator−core and stem III helices could exist simultaneously. Their incompatibility arises from geometric constraints and from the rigidity of A-form helices. The added length and flexibility conferred by two or five single-stranded nucleotides at either end of the antisense does not interfere with attenuation or activation, while 10 nucleotides of single strandedness appears to allow simultaneous formation of all three helices and to prevent activation by the sense strand oligo.

In general, a practical upper limit on antisense length could arise either from increases in the conformational flexibility in single-stranded regions or from the increasing likelihood that self-structure in long antisense sequences (or their targets) may lead to structural interference. TRAP construct HH8(A+10).8, which carries a 30-nt antisense, is attenuated to the greatest degree among all constructs that carry an 8-nt attenuator. Neither of the 20-nt activator oligos (8A and 8A*10) rescued the cleavage activity to detectable levels (Table 3), while pairing of the 30-nt oligo 8A+10 restored cleavage activity to approximately 10% of the maximal rate.

The 25-nt antisense segment in HH8(A+5).8 may be close to optimal. Its unactivated cleavage rate is at the minimum of our detection level, but addition of RNA oligo 8A or 8A*5 activated this ribozyme by 555- or 733-fold, respectively. This is two to three times the activation observed for HH8A.8 and HH8(A+2) and several related constructs (Table 3) (*7*). The observation that a TRAP with 25 or 30 nucleotides in the antisense is more severely attenuated than one with 20 nucleotides suggests that the shorter antisense places limitations on attenuation. The antisense may resist being stretched to its full extent to allow the attenuator to find the core and thereby contribute positive ΔG to the attenuated conformation. The enhanced attenuation observed with HH8(A+5).8 is an important factor leading to its extraordinary activation.

Application to TRAP Ribozyme Design. A well-regulated TRAP ribozyme is a potential candidate for modulating gene expression in vivo. The antisense sequences of ribozymes examined thus far have low propensity for forming structure other than the intended duplex with the activator. This simplified system is highly useful for working out the fundamental principles of the TRAP design. Real antisense sequences, however, could contain internal structures that interfere with binding to the sense strand or with ribozyme folding. A combination of computational structure prediction and screening of candidate ribozyme constructs should permit application of the TRAP design to biologically relevant sequences.

For some cleavage targets, high ribozyme activity will be required to achieve a biological effect. These may readily tolerate appreciable background cleavage activity in the attenuated state while requiring vigorous cleavage in the activated state. This behavior is exemplified by HH8A.8 (0.0024 vs 0.65 min^{-1}, Table 1). Other cleavage targets will exhibit a biological response upon very modest reductions in their intracellular concentrations. Ribozymes for these targets should be kept more rigorously turned off in their attenuated states so as not to disrupt nontarget cells, and may be fully adequate if activated to a small fraction of the maximal rate of RNA cleavage. This behavior is exemplified by HH8(A+10).8 (<0.0004 vs 0.13 min^{-1}). The parameters described above will help guide the design of biologically active TRAPs with the appropriate activities in their repressed and activated forms.

ACKNOWLEDGMENT

We thank Manami Saha and Amy Boles for critical comments on the manuscript.

REFERENCES

1. Breaker, R. (2002) Engineered allosteric ribozymes as biosensor components. *Curr. Opin. Biotechnol. 13*, 31−39.
2. Silverman, S. (2003) Rube Goldberg goes (ribo)nuclear? Molecular switches and sensors made from RNA. *RNA 9*, 377−383.
3. Frauendorf, C., and Jaschke, A. (2001) Detection of small organic analytes by fluorescing molecular switches. *Bioorg. Med. Chem. 9*, 2521−2524.
4. Sekella, P., Rueda, D., and Walter, N. (2002) A biosensor for theophylline based on fluorescence detection of ligand-induced hammerhead ribozyme cleavage. *RNA 8*, 1242−1252.
5. Liu, J., and Lu, Y. (2002) FRET study of a trifluorophore-labeled DNAzyme. *J. Am. Chem. Soc. 124*, 15208−15216.
6. Tanabe, T., Kuwabara, T., Warashina, M., Tani, K., Taira, K., and Asano, S. (2000) Oncogene inactivation in a mouse model. *Nature 406*, 473−474.
7. Burke, D. H., Ozerova, N. D. S., and Nilsen-Hamilton, M. (2002) Allosteric hammerhead TRAP ribozymes. *Biochemistry 41*, 6588−6594.
8. Cantor, C., and Schimmel, P. R. (1980) in *Biophysical Chemistry*, p 1132, W. H. Freeman and Co., New York.
9. Marky, L. A., and Breslauer, K. J. (1987) Calculating thermodynamic data for transitions of any molecularity from equilibrium melting curves. *Biopolymers 26*, 1601−1620.
10. Fedor, M. J., and Uhlenbeck, O. C. (1990) Substrate sequence effects on "hammerhead" RNA catalytic efficiency. *Proc. Natl. Acad. Sci., U.S.A. 87*, 1668−1672.
11. Fedor, M., and Uhlenbeck, O. (1992) Kinetics of intermolecular cleavage by hammerhead ribozymes. *Biochemistry 31*, 12042−12054.
12. Hertel, K., Herschlag, D., and Uhlenbeck, O. (1994) A kinetic and thermodynamic framework for the hammerhead ribozyme reaction. *Biochemistry 33*, 3374−3385.

13. Stage-Zimmermann, T. K., and Uhlenbeck, O. C. (1998) Hammerhead ribozyme kinetics. *RNA 4*, 875−889.
14. Hall, K. B., and McLaughlin, L. W. (1991) Thermodynamic and structural properties of pentamer DNA·DNA, RNA·RNA, and DNA·RNA duplexes of identical sequence. *Biochemistry 30*, 10606−10613.
15. Lesnik, E. A., and Freier, S. M. (1995) Relative thermodynamic stability of DNA, RNA, and DNA:RNA hybrid duplexes: relationship with base composition and structure *Biochemistry*, *34*, 10807−10815.
16. Sugimoto, N., Nakano, S., Katoh, M., Matsumura, A., Nakamuta, H., Ohmichi, T., Yoneyama, M., and Sasaki, M. (1995) Thermodynamic parameters to predict stability of RNA/DNA hybrid duplexes. *Biochemistry 34*, 11211−11216.
17. Gray, D. M. (1997) Derivation of nearest-neighbor properties from data on nucleic acid oligomers. II. Thermodynamic parameters of DNA·RNA hybrids and DNA duplexes. *Biopolymers 42*, 795−810.

BI034960K